Supplementary Information for "Efficient Spin-Orbit Torque Switching in a Magnetic Insulator via Ultrathin Pt and Light Metal Overlayers"

Stefano Fedel[1*] and Can O. Avci[1]

[1]*Institut de Ciencia de Materials de Barcelona (ICMAB-CSIC), Bellaterra, Spain 08193.*

E-mail: sfedel@icmab.es

Supplementary Note 1: Measurements on TbIG/Cu/Pt Structures

To investigate the role of the TbIG/Pt interface, we fabricated additional samples with a Cu spacer inserted between Pt (1.2 nm) and TbIG. Figure S1A shows the longitudinal resistance and a schematic of the stack. The anomalous Hall resistance R_{AHE} (black, left axis) and the normalized R_{AHE}/R_{xx} (red, right axis) in Fig. S1B both exhibit a linear decrease, similar to the behavior observed in Pt/Ti bilayers. As expected for Cu, a light metal, no AHE signal originates from the spacer.

Figure S1C presents the critical current I_c (black, right axis) and the corresponding current density j_c (red, left axis). Although the Cu layer is expected to be spin-transparent and non-contributing to SOT, a reduction in j_c by approximately a factor of two is observed for both Cu (1.5 nm) and Cu (3 nm) spacers. This suggests that the Cu/Pt interface may enhance spin scattering and improve spin current injection. The similar behavior for both Cu thicknesses implies that the Cu spacer remains transparent to spin currents as long as

it is sufficiently thin. Furthermore, contributions from the TbIG/Pt interface seem to be negligible.

The power dissipated during switching is shown in Fig. S1D, with a slight increase for Cu (1.5 nm) and a return to baseline for Cu (3 nm).

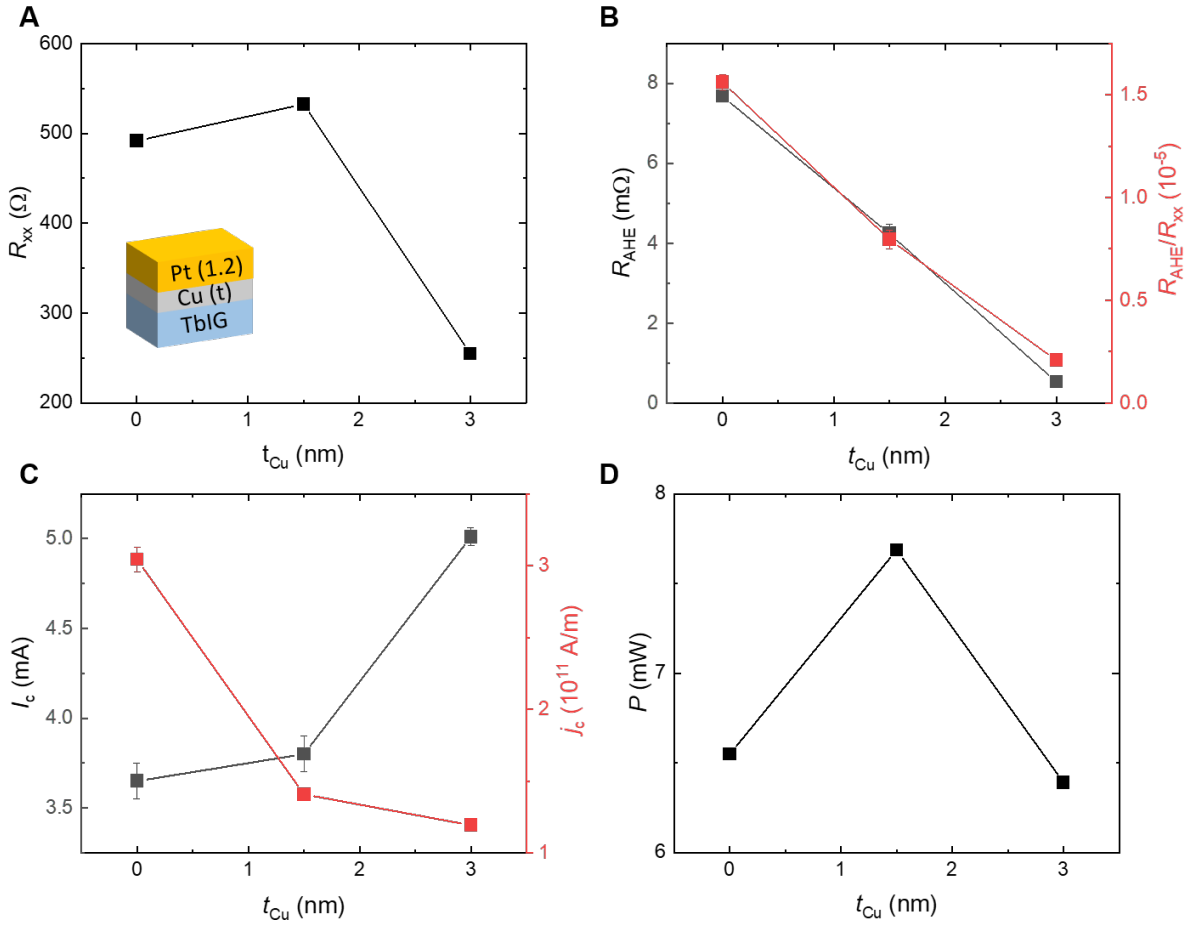

Figure S1: **Analysis of TbIG/Cu(t)/Pt(1.2nm) heterostructures.** (A) Longitudinal resistance of TbIG/Cu(t)/Pt(1.2 nm) trilayers and corresponding stack schematic. (B) Anomalous Hall resistance R_{AHE} (left axis, black) and normalized R_{AHE}/R_{xx} (right axis, red). (C) Critical switching current I_c (right axis, black) and current density j_c (left axis, red). (D) Power dissipated during switching.

Supplementary Note 2: Pt Thickness Calibration by XRR

Pt layers were calibrated by X-ray reflectometry (XRR) on SiO_x substrates with deposition times of 65 s, 130 s, and 390 s, corresponding to thicknesses of 5.2, 9.9, and 30.4 nm,

respectively (Fig. S2A to C). These yield deposition rates of 0.080, 0.076, and 0.080 nm/s, confirming a consistent average rate of 0.0786 nm/s, slightly above the previous estimate (0.078 nm/s). For a deposition time of 7.8 s (used for 0.6 nm Pt), this results in a thickness of 0.61 nm, within the accuracy of the sputtering system. The linear calibration is shown in Fig. S2D.

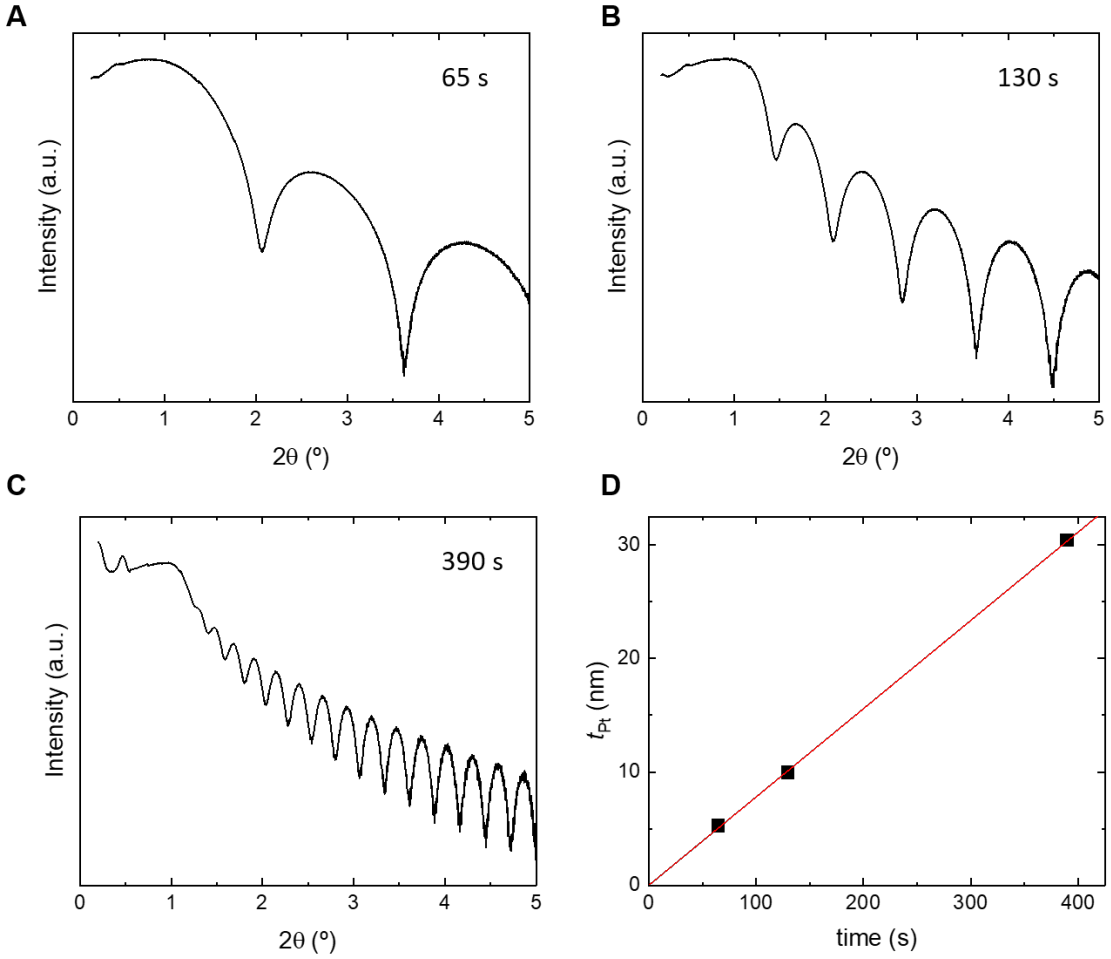

Figure S2: **XRR calibration of Pt thickness.**
XRR data for Pt films deposited on SiO_x with deposition times of 65 s (A), 130 s (B), and 390 s (C). (D) Linear fit of deposition time vs. extracted Pt thickness.

Supplementary Note 3: Surface Characterization of TbIG/Pt

Atomic force microscopy scans of TbIG/Pt (0.6 nm), and TbIG/Pt (1.2 nm) are shown in Fig. S3. Both samples exhibit similar surface roughness (∼100 pm RMS) and morphology within the measurement resolution, suggesting that the granular structure of ultrathin Pt cannot be resolved by AFM.

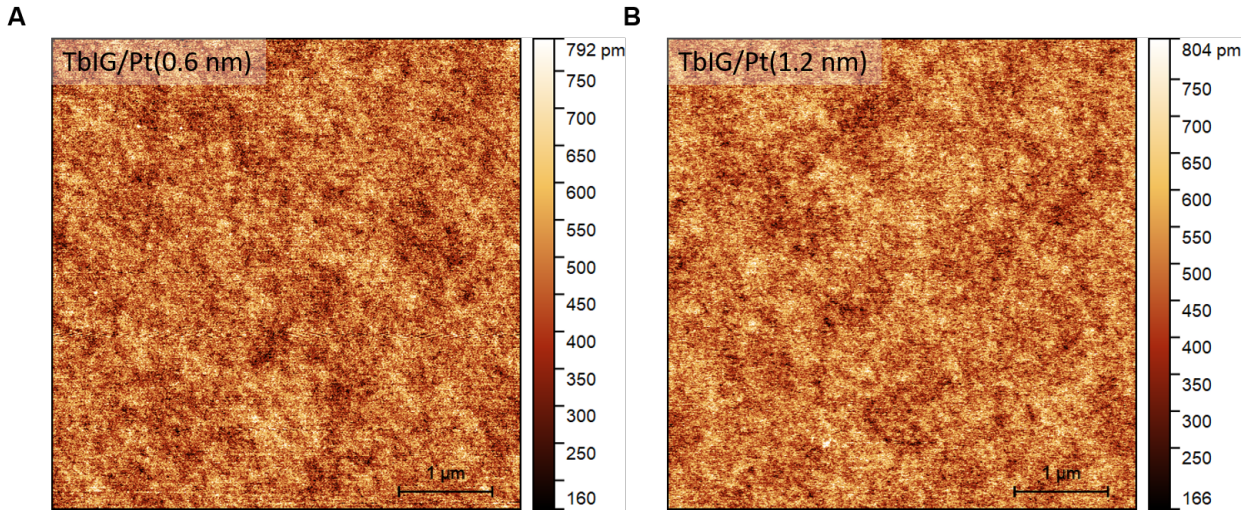

Figure S3: **AFM scans of TbIG/Pt.**
AFM scans of (A) TbIG, (B) TbIG/Pt (0.6 nm), and (C) TbIG/Pt (1.2 nm), all showing flat surfaces with comparable RMS roughness.

Supplementary Note 4: Comparison Between OOP Hysteresis Loop and Nanosecond Switching Signal

Figure S4 compares the MOKE signal of an out-of-plane magnetic field scan (A) and one branch of the nanosecond-pulse switching loop (B) for TbIG/Pt (0.6 nm). The signals were measured under identical conditions. The MOKE intensity difference between up/down states (∼160) is the same in both, confirming full magnetization reversal even in the presence of nanogranular Pt.

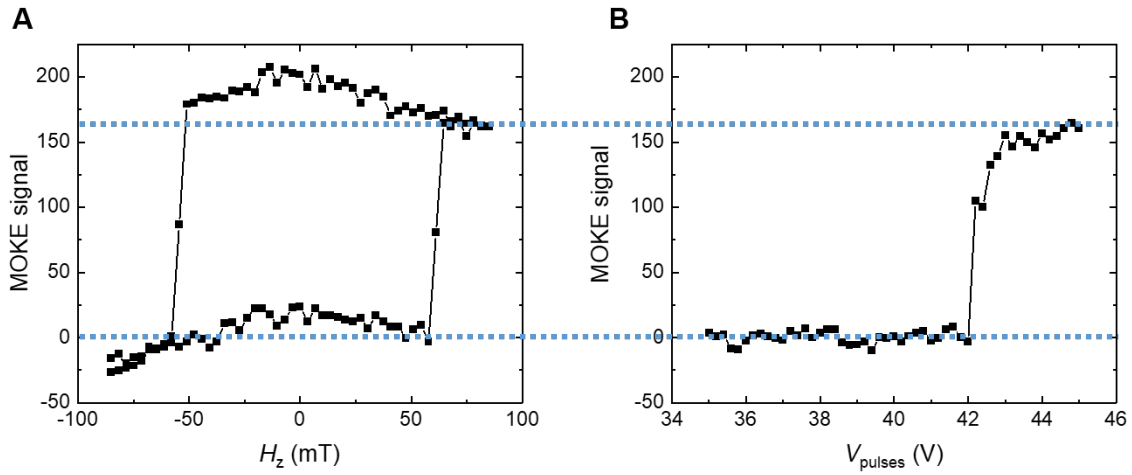

Figure S4: **MOKE signal intensity for OOP hysteresis loop and SOT switching.** (A) Magnetic field hysteresis loop and (B) nanosecond pulse switching branch for TbIG/Pt (0.6 nm). Identical MOKE intensity confirms full switching.

Supplementary Note 5: TbIG/Pt(0.6 nm)/Ti(7 nm)

Figure S5 shows the Hall measurement of the sample TbIG/Pt (0.6 nm)/Ti (7 nm). Only the ordinary Hall effect is visible; no AHE signal or SOT-induced switching (not shown) is observed. This indicates that 0.6 nm of Pt is insufficient to prevent intermixing between TbIG and Ti, degrading the magnetic properties and the TbIG/Pt interface required for AHE and SOT switching.

Supplementary Note 6: Parallel Resistor Model

The total resistance of TbIG/Pt (1.2 nm)/Ti(t) samples was fitted with an exponential decay to estimate the resistance of the Pt layer, yielding $R_{\mathrm{Pt}} \approx 1737\ \Omega$ (Fig. S6A).

Assuming a parallel resistor model:

$$\frac{1}{R_{\mathrm{tot}}} = \frac{1}{R_{\mathrm{Pt}}} + \frac{1}{R_{\mathrm{Ti}}}, \tag{1}$$

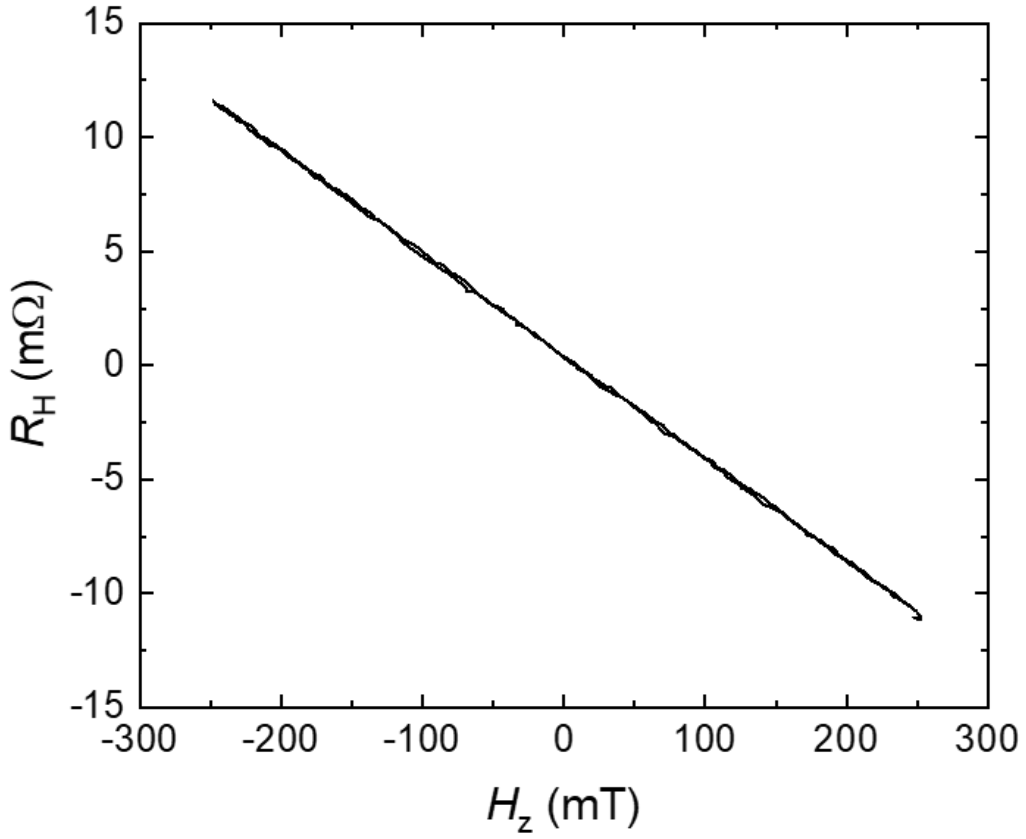

Figure S5: **Hall measurement for TbIG/Pt(0.6 nm)/Ti(7 nm).**
Hall measurement for TbIG/Pt(0.6 nm)/Ti(7 nm) shows only the OHE, with no sign of AHE.

we calculated R_{Ti} for different Ti thicknesses. The current in each layer is estimated as:

$$I_{\mathrm{Ti(Pt)}} = \frac{I_{\mathrm{tot}} R_{\mathrm{tot}}}{R_{\mathrm{Ti(Pt)}}}. \tag{2}$$

The extracted resistivity of Ti (Fig. S6C) matches literature values for sputtered Ti films.[1]

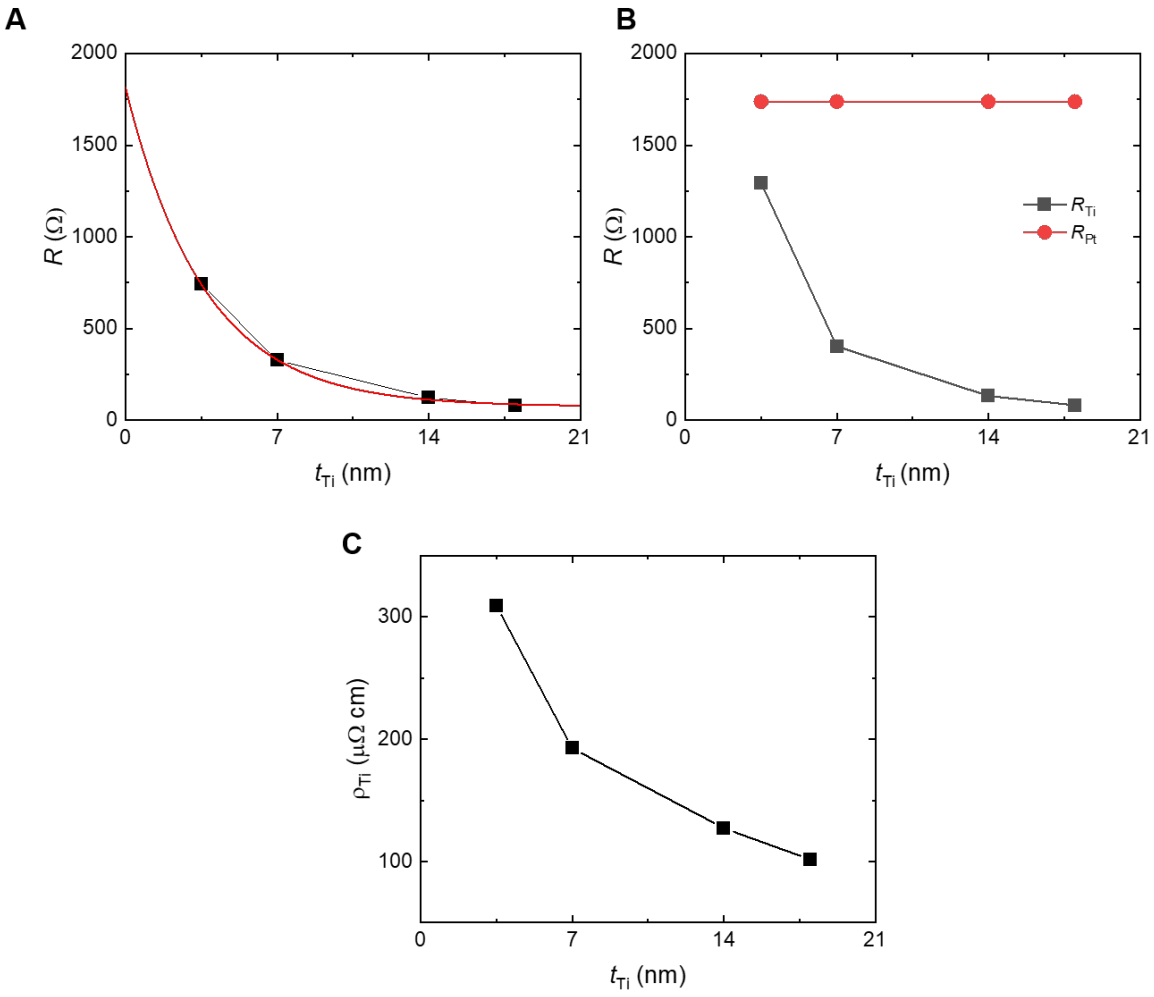

Figure S6: **Estimation of current distribution in Pt/Ti bilayers and Ti resistivity.** (A) Total longitudinal resistance of TbIG/Pt (1.2 nm)/Ti(t) stack. (B) Resistance of Ti layer estimated using a parallel resistor model. (C) Extracted resistivity of Ti as a function of Ti thickness.

Supplementary Note 7: I–V Curves of TbIG/Pt Samples

Figure S7 shows the I–V curves for Pt (0.6 nm) and Pt (0.75 nm). Both exhibit linear Ohmic behavior, confirming that charge transport in ultrathin Pt is not dominated by hopping or tunneling between isolated islands.

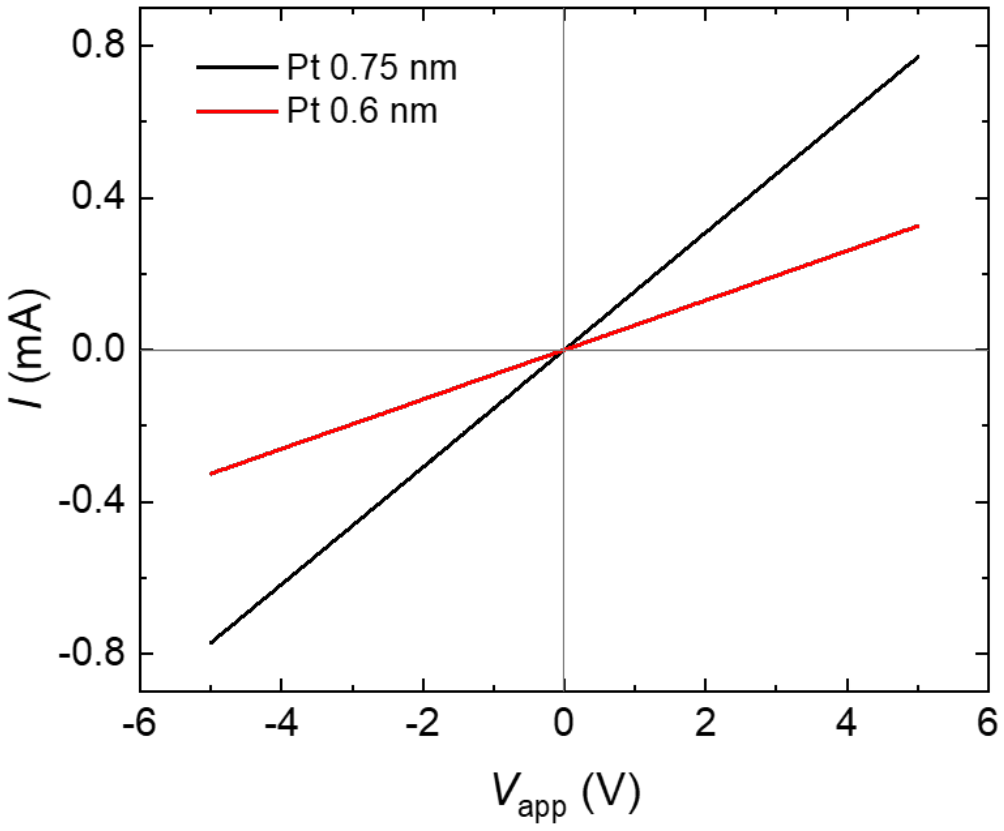

Figure S7: **I–V curves of ultrathin Pt.**
I–V curves of TbIG/Pt (0.6 nm, red) and TbIG/Pt (0.75 nm, black). Linear behavior indicates Ohmic conduction.

References

(1) Korotkova, K.; Bainov, D.; Smirnov, S.; Yunusov, I.; Zhidik, Y. Electrical conductivity and optical properties of nanoscale titanium films on sapphire for localized plasmon

58 resonance-based sensors. *Coatings* **2020**, *10*, 1165.